Dalton Transactions

An international journal of inorganic chemistry

Accepted Manuscript

This article can be cited before page numbers have been issued, to do this please use: M. Lucic, A. K. Chaplin, T. Moreno-Chicano, F. Dworkowski, M. Wilson, D. Svistunenko, M. Hough and J. A.R. Worrall, *Dalton Trans.*, 2020, DOI: 10.1039/C9DT04583J.

ROYAL SOCIETY OF CHEMISTRY

rsc.li/dalton

A subtle structural change in the distal haem pocket has a remarkable effect on tuning hydrogen peroxide reactivity in dye decolourising peroxidases from *Streptomyces lividans*

Marina Lučić,[1] Amanda K. Chaplin,[1†] Tadeo Moreno-Chicano,[1§] Florian S.N. Dworkowski,[2] Michael T. Wilson,[1] Dimitri A. Svistunenko,[1] Michael A. Hough,[1] Jonathan A.R. Worrall[1]

[1]School of Life Sciences, University of Essex, Wivenhoe Park, Colchester, CO4 3SQ, UK.
[2]Swiss Light Source, Paul Scherrer Institute, Villigen PSI, CH-5232, Switzerland.

Current address: [†]Department of Biochemistry, Sanger Building, 80 Tennis Court Road, Cambridge CB2 1GA, UK. [§]Institut de Biologie Structurale, 71 Avenue des Martys, 38000 Grenoble, France.

View Article Online
DOI: 10.1039/C9DT04583J

ABSTRACT

Dye decolourising peroxidases (DyPs) are oxidative haem containing enzymes that can oxidise organic substrates by first reacting with hydrogen peroxide. Herein, we have focused on two DyP homologs, DtpAa and DtpA, from the soil-dwelling bacterium *Streptomyces lividans*. By using X-ray crystallography, stopped-flow kinetics, deuterium kinetic isotope studies and EPR spectroscopy, we show that both DyPs react with peroxide to form Compound I (a Fe^{IV}=O species and a porphyrin π-cation radical), via a common mechanism, but the reactivity and rate limits that define the mechanism are markedly different between the two homologs (DtpA forms Compound I rapidly, no kinetic isotope effect; DtpAa 100-fold slower Compound I formation and a distinct kinetic isotope effect). By determining the validated ferric X-ray structure of DtpAa and comparing it with the ferric DtpA structure, we attribute the kinetic differences to a subtle structural repositioning of the distal haem pocket Asp side chain. Through site-directed mutagenesis we show the acid-base catalyst responsible for proton-transfer to form Compound I comprises a combination of a water molecule and the distal Asp. Compound I formation in the wild-type enzymes as well as their distal Asp variants is pH dependent, sharing a common ionisation equilibrium with an apparent pK_a of ~ 4.5-5.0. We attribute this pK_a to the deprotonation/protonation of the haem bound H_2O_2. Our studies therefore reveal a mechanism for Compound I formation in which the rate limit may be shifted from peroxide binding to proton-transfer controlled by the distal Asp position and the associated hydrogen-bonded water molecules.

View Article Online
DOI: 10.1039/C9DT04583J

INTRODUCTION

Iron-containing enzymes can utilise oxygen to carry out a variety of oxidative transformations.[1] In the case of haem peroxidases, their interaction with H_2O_2 leads to the formation of two iron(IV)-oxo intermediates, commonly referred to as 'ferryl' haem species and are the active forms in the catalytic cycle.[2, 3] Prior to formation of the first ferryl haem intermediate, H_2O_2 binds to the ferric haem and undergoes heterolytic scission of the O-O bond to form Compound I, which comprises of a Fe^{IV}=O species and a porphyrin π-cation radical, [(Fe^{IV}=O)por•+].[4] Reduction of the porphyrin π-cation radical occurs in a single-electron step by an electron supplied by a reducing substrate to yield the second ferryl haem intermediate, Compound II (Fe^{IV}=O or Fe^{IV}-OH if protonated).[2, 3] A further one-electron reduction of Compound II returns the haem to the ferric state.[2, 3] In addition to peroxidases a large number of haem enzymes (e.g. P450s, NO synthase and catalases) use ferryl haem as part of their catalytic mechanism and thus much effort has been focused on understanding the formation, nature and reactivity of ferryl haem.[5, 6]

Dye decolourising peroxidases (DyPs) are the most recent family of haem peroxidases to be discovered[7] and are now known to be widely distributed in bacterial and fungal genomes.[8] The name given arises from the initial recognition of an ability to efficiently catalyse the decolourisation of bulky industrial dyes such as anthraquinone derivatives.[7] Whilst it is now recognised that DyPs have a broad substrate specificity, knowledge of their physiological substrates is lacking. However, a recent report has identified an anti-fungal anthraquinone based compound as a substrate for a DyP from the fungus *Bjerkandera adusta*.[9] Based on phylogenetic and structural analysis, DyPs have been placed into three sub-families (types A, B, C/D), which differ predominately in their cellular location, structure and enzymatic activity.[8, 10-12] From a structural perspective, DyPs are distinct from the α-helical fold of members from other peroxidase classes, such as yeast cytochrome c peroxidase (CcP)[13] and horse radish peroxidase (HRP)[14] and instead comprise a two domain α + β ferredoxin-like fold.[15]

A distinguishing feature of the DyP family is the absence of a distal haem pocket His residue, which in nonmammalian peroxidases such as HRP, ascorbate peroxidase (APX) and CcP is part of a highly conserved His-Arg couple that plays a prominent role in Compound I formation.[16-18] The distal His functions as an acid-base catalyst, removing the proton from the O^{α} atom of the bound Fe^{III}-O_2H_2,[19, 20] to generate an anionic precursor to Compound I known as Compound 0 (Fe^{III}-O^{α}–O^{β}H).[21, 22] The proton is then transferred to the O^{β} atom of

Compound 0 to form an oxy-water complex (Fe^{III}-O-OH_2) that enables the distal oxygen to leave as a H_2O molecule.[19, 20] Thus, heterolysis of the O-O bond is proton assisted. In DyPs a distal Asp-Arg couple is present,[15] with the recently identified exception being the DyP from *Cellulomonas bogoriensis* where a Glu replaces the Asp.[12] Compound I formation in some DyPs argue for the distal Arg being the proton acceptor and donor,[23, 24] whereas in others the Asp has been reported to serve as the acid-base catalyst.[25, 26]

The genome of the soil-dwelling Gram positive bacterium *S. lividans* contains three genes encoding for DyPs. Two of these are A-types, DtpA and DtpAa, and are secreted to the extracytoplasmic environment, with the third, a B-type (DtpB), located in the cytoplasm. Detailed structural and mechanistic characterisation of DtpA have revealed it can rapidly react with H_2O_2 to form Compound I with a second-order rate constant of 8.9 x 10^6 M^{-1} s^{-1} and turnover anthraquinone dyes as well as conventional peroxidase substrates.[27, 28] Intriguingly, DtpA has been implicated to function in a copper trafficking pathway in *S. lividans*, where it is postulated to react in the pathway with the H_2O_2 produced from the radical copper oxidase, GlxA.[29] As of yet no mechanistic characterisation of DtpAa has been reported, but a recent serial femtosecond crystallography study using an X-ray free electron laser (XFEL) approach has determined the DtpAa structure at room temperature with the haem in the ferric oxidation state.[30] A key factor for the interpretation of structure/mechanism studies with metalloproteins and enzymes is to ensure that the structures determined are in the redox state generated prior to exposure by X-rays. In the case of peroxidases several strategies have been employed to ensure the redox state of the haem is validated including the metastable Compound I and Compound II intermediates of the peroxidase reaction cycle.[31-37]

Insights into why *S. lividans* possesses two A-type DyP homologs in the same cellular location and to their biological function, can begin to be addressed through structure and mechanistic studies. Herein we have determined the validated cryo-cooled X-ray structure of DtpAa in the ferric haem state, enabling comparison of the distal haem pocket with the room temperature XFEL structure[30] and importantly with the recently determined ferric DtpA structure.[28] To elucidate the mechanistic features on reaction with H_2O_2, stopped-flow reaction kinetics, including deuterium kinetic isotope exchange experiments, pH dependency of Compound I formation, EPR spectroscopy and site-directed mutagenesis to create the distal Asp mutants of DtpAa and DtpA have been performed. Our data conform to a common mechanism for Compound I formation in DtpAa and DtpA, but remarkably, despite identical distal haem pockets in the two DyPs, the rate limits of H_2O_2 reactivity are tuned by a subtle positional shift in the side chain of the distal pocket Asp.

View Article Online
DOI: 10.1039/C9DT04583J

EXPERIMENTAL

Site-directed mutagenesis of DtpAa and DtpA

A pET28a vector (Novagen) containing the nucleotide sequence encoding for residues 48 to 420 of DtpAa and residues 69 to 445 of DtpA served as the template for site-directed mutagenesis using the QuikChange protocol (Stratagene). The following forward and reverse primers to create the D239A mutant and the D251A mutant of DtpAa and DtpA, respectively, were designed and synthesized (Sigma); D251A-F 5'-GCCAGGTCGCCGGCACCCGCAAC-3', D251A-R 5'-GTTGCGGGTGCCGGCGACCTGGC-3', 5'-D239A-F GGCTTCAAGGCCGGCACCCGCAAC-3', 5'-D239A-R CCGAAGTTCCGGCCGTGGGCGTTG-3'. A polymerase chain reaction (PCR) mix consisting of the respective primers (75 ng/μL), the respective pET28a template (15 ng/μL), 10 mM dNTPs (Fermentas), *Pfu* Turbo polymerase (Agilent), 10 x *Pfu* buffer (Agilent) and deionised water was prepared and subjected to the following PCR cycle; 95 ^{o}C for 3 min; 18 cycles of 95 ^{o}C for 1 min, 65 ^{o}C for 1 min and 72 ^{o}C for 8 min; and 72 ^{o}C for 10 min. Clones were corroborated for the presence of the desired mutation by DNA sequencing (Source Bioscience).

Purification of DtpAa and DtpA

DtpAa and DtpA were over-expressed in *Escherichia coli* BL21(DE3) cells and purified as previously reported.[29, 30] Following purification both DtpAa and DtpA were stored at -20 ^{o}C in 50 mM sodium acetate pH 5.0, 100 mM NaCl. The D239A and D251A variants were over-expressed and purified in an identical manner to their respective wild-type protein.

Sample preparation

Concentrations of purified DtpAa and DtpA, as well as variants were determined spectrophotometrically using a Cary 60 UV-visible spectrophotometer (Agilent) and an extinction coefficient (ε) at 280 nm of 46,057 M^{-1} cm^{-1} for DtpAa and 37,470 M^{-1} cm^{-1} for DtpA. Buffers used were 50 mM sodium acetate pH 5.0, 150 mM NaCl; 20 mM sodium phosphate 100 mM NaCl, pH 7.0 and a mixed buffer system comprising of 10 mM Tris, 10 mM MES, 10 mM MOPS, 10 mM sodium acetate, 200 mM potassium chloride with the pH adjusted between values of 4 and 10 as required. Enzymes were exchanged into a desired buffer using a PD-10 column (Generon) and concentrated using centrifugal ultrafiltration devices

(Vivaspin GE Healthcare). H_2O_2 solutions (Sigma-Aldrich) were prepared from a stock with the final concentration determined spectrophotometrically using an $\varepsilon = 43.6\ M^{-1}\ cm^{-1}$ at 240 nm.[38] The required deuterated buffers were prepared in 99.9% D_2O (Sigma). Highly concentrated enzymes and H_2O_2 stocks were diluted directly in D_2O and left to equilibrate in the D_2O solutions before analysis.

Stopped-flow absorption kinetics

Transient kinetics of the interaction of H_2O_2 with ferric enzymes was performed using a SX20 stopped-flow spectrophotometer (Applied Photophysics) equipped with either a photomultiplier or a diode-array multi-wavelength unit and thermostatted to 25 ^oC. Enzyme solutions (10 μM before mixing) were prepared in the appropriate buffer (H_2O or D_2O) and mixed with a series of H_2O_2 (or D_2O_2) concentrations (ranging from 4 – 10,000 μM before mixing, depending on enzyme used). The overall spectral transitions were monitored using either the photomultiplier or diode array unit and fitted to models in the Pro-K software (Applied Photophysics) to yield rate constants for Compound I (k_{obs1}) and Compound II formation (k_{obs2}). Rate constants for Compound I formation (k_{obs1}) at various pH values were obtained using 10 μM of enzyme (before mixing) and a fixed H_2O_2 concentration, which for DtpA was 50 μM, DtpAa 250 μM, D251A 500 μM and D239A 250 μM (all after mixing).

Preparation of DtpAa time course samples for EPR measurements

A time series of DtpAa samples following activation by H_2O_2 was created in two ways. The first procedure required the addition of a stock solution of H_2O_2 (~10 mM) to a DtpAa sample (40 μM) to give a 1:10 ratio (DtpA:H_2O_2), from which an aliquot was drawn and frozen in methanol kept on dry ice (~195 K). This method provided the freezing time (*i.e.* the reaction time) from 11 s and upwards. The second procedure to enable sub 10 s sample preparation required the stock H_2O_2 solution to be inserted into plastic tubing connected to the syringe used to draw the DtpAa sample from the EPR tube, which was subsequently loaded back to the EPR tube and frozen, providing freezing times from 4 s.

EPR spectroscopy and simulation

Wilmad SQ EPR tubes (Wilmad Glass, Buena, NJ) with OD = 4.05 ± 0.07 mm and ID = 3.12 ± 0.04 mm (mean ± range) were used. Samples frozen in a set of these tubes yielded very similar intensities of EPR signals; with only ~1-3% random error. All EPR spectra were

measured on a Bruker EMX EPR spectrometer (X-band) at a modulation frequency of 100 kHz. A Bruker resonator ER 4122 (SP9703) and an Oxford Instruments liquid helium system were used to measure the low-temperature (10 K) EPR spectra. EPR spectra of a blank sample (frozen water) measured at the same set of instrumental conditions were subtracted from the DtpAa spectra to eliminate the background baseline EPR signal. Spectra deconvolution into two components and measurements of the intensities of these components in the time dependence set of samples were performed by using the procedure of spectra subtraction with variable coefficient.[39] Quantitative estimates of the concentrations of the paramagnetic centres were performed by comparison of the second integrals simulated EPR signals with a reference to known total concentration of the ferric haem in the sample. The simulation was performed by WinEPR SimFonia (Bruker).

Crystallisation, microspectrophotometry and X-ray data collection strategy

Crystals of ferric DtpAa (3 – 6.5 mg/ml) grew under batch conditions in a solution of 100 mM HEPES, 20% PEG 6000 (Sigma) pH 7.0 and were cryo-protected in a 40% w/v sucrose (Fisher) solution and flash-cooled in liquid nitrogen. X-ray diffraction and single crystal spectroscopic data at 100 K were collected at the Swiss Light Source (SLS) beamline X10SA. The MS3 on-axis microspectrophotometer[40] was used to measure absorbance spectra of ferric DtpAa crystals in the range of 450 to 700 nm. Each spectrum was the result of 50 accumulations of 100 ms exposures. Spectra were measured prior to and following X-ray data collection and a dose limit was selected such that minimal changes occurred to the spectrum of the ferric form during data collection from each crystal.

X-ray structure determination and refinement

A multi-crystal approach was performed to obtain a complete low-dose composite dataset for the ferric DtpAa structure. A total of 13 spectroscopically-validated diffraction data wedges were merged using the in house go2gether.com script in the XDS package.[41] The ferric DtpAa structure was refined from a starting model of the serial femtosecond crystallography room temperature structure of DtpAa (pdb code 6I43).[30] Refinement of the structure was carried out initially using Refmac5[42] in the CCP4 suite and subsequently in PHENIX,[43] with model building between refinement cycles in Coot.[44] Riding hydrogen atoms were added during refinement. The structure was validated using the Molprobity server,[45] the JCSG Quality Control Server and tools within Coot.[44] A summary of data collection and refinement statistics are given in Table 1. X-ray absorbed dose was estimated using Raddose-3D.[46] To reflect the

beam profile used, a weighted average of doses calculated for top hat and Gaussian profiles was calculated and doses were estimated for the range of crystal dimensions used. Estimates of bond length error for the iron-water and iron-proximal His bonds were derived using the Online_DPI server[47] based on the estimated coordinate error as previously described.[48]

RESULTS

The electronic absorbance spectrum of DtpAa

The electronic absorbance spectrum of purified DtpAa at pH 7.0 is shown in Fig. 1A, with the peak maxima wavelengths reported in Table 2, alongside those of DtpA for comparison. The spectrum is consistent with a high-spin (HS) ferric haem species, which upon addition of one-equivalent H_2O_2, leads to a decrease in the Soret band intensity and a red shift in wavelength, coinciding with the appearance of α and β bands of equal intensity and a further low intensity charge transfer band in the red region (Fig, 1A and Table2). No further changes to the spectrum are observed on subsequent additions of H_2O_2. Comparison with the wavelength maxima of the high-valent haem intermediates generated during the peroxidase cycle in DtpA *i.e.* Compound I ([$(Fe^{4+}=O)por^{\bullet+}$]) and Compound II ($Fe^{4+}=O$ or Fe^{4+}-OH) (Table 2),[27, 29] suggests the spectrum generated on addition of H_2O_2 to DtpAa is consistent with a Compound II species. We have previously reported that on stoichiometric addition of H_2O_2 to DtpA, a Compound I absorbance spectrum forms.[27] Therefore in contrast for DtpAa, Compound II forms without any detectable Compound I formation in the static absorbance experiment, suggesting the possibility of an unstable Compound I species that decays rapidly to Compound II (*vide infra*).

Validation of the ferric haem state in the crystal structure of DtpAa

To compare the structures of DtpAa and DtpA, determined by X-ray crystallography, it is important that the oxidation state of the haem in the structure is validated. The spectroscopically-validated X-ray crystal structure of ferric DtpA has been determined previously.[28] Prior to X-ray diffraction data collection, an absorbance spectrum at 100 K of a DtpAa crystal was acquired using the on-axis UV-vis microspectrophotometer at the SLS (Fig. 1B). Identical electronic absorbance bands to those of the ferric DtpAa in solution are observed (Fig. 1B and Table 2), indicating a ferric DtpAa species in the crystal. On exposure to X-rays, dose-dependent changes in the electronic absorbance spectrum of the crystal were observed, consistent with reduction of the haem iron to a ferrous state. Therefore, to mitigate against this X-ray induced photo-reduction of the ferric DtpAa crystal, a multi-crystal strategy was employed whereby 20° wedges (a total of 200 images each of 0.1° oscillation) were collected

per ferric DtpAa crystal (or position on a larger crystal). Absorbance spectra were recorded prior to and following the measurement of each data wedge and examined to ensure that the spectrum of the ferric form remained largely intact (Fig. 1B). Each wedge was merged to create a composite data set culminating in an overall dose of between 17.0 and 21.7 kGy, for crystals in the range 50-100 μm in size, as outlined in the Experimental section, producing a crystallographic data set of a close-to-intact ferric species.

Comparison of the ferric DtpAa and DtpA X-ray structures determined at 100 K

The validated ferric DtpAa X-ray structure was determined to 1.80 Å resolution (Table 1), with two DtpAa monomers (chains A and B) found in the crystallographic asymmetric unit (all bond-lengths and B-factors reported herein refer to chain A). Electron density was visible for residues 55-416 in chain A and 56-417 in chain B. The overall monomer fold of DtpAa consists of two ferredoxin-like folds (composed of βαββαβ secondary structure), to create two domains in which one houses the *b*-type haem (Fig. 2A). A comparison of the tertiary structures of DtpAa and DtpA illustrates the structural homology of the core βαββαβ fold between these two A-type DyPs, with changes in helical content and loop insertions and/or deletions contributing to the variation in structural shape (Fig. 2A). Most notable are two extended loop sections incorporating residues 113 and 125 in DtpAa and residues 337 and 347 in DtpA (Fig. 2A and Fig. S1 reporting a primary sequence alignment).

The ferric haem in DtpAa is six-coordinate, with axial coordination from a proximal His residue, (His326 $N^{\delta1}$-Fe bond 2.19 ± 0.13 Å) and a distal H_2O (w1) molecule (B-factor 12.6 $Å^2$) (Fig. 2B). The distal Fe(III)-OH_2 bond length (2.32 ± 0.13 Å) is significantly longer in DtpAa compared to in DtpA (1.98 ± 0.096 Å, B-factor 11.5 $Å^2$), despite the ferric nature of the haem in both structures. The highly conserved distal haem pocket residues, Asp239 and Arg342, participate in several hydrogen-bonding (H-bonding) interactions, including to each other and in the case of Arg342 to the haem propionate-6 (Fig. 2B). Of particular note is that the $O^{\delta1}$ atom of Asp239 H-bonds (2.72 Å) with w1 in the ferric DtpAa structure (red-dashed line Fig. 2B). This H-bonding interaction is absent in ferric DtpA, where a distance of 4.15 Å from the $O^{\delta1}$ atom of Asp251 and w1 is observed (Fig. 2B). In DtpAa a clear positional shift in the side chain of Asp239 towards the haem is apparent, permitting the H-bonding interaction with w1, and may concomitantly assist in lengthening the Fe-OH_2 distal bond-length (Fig. 2B). Therefore, in DtpAa, the distal H_2O is H-bonded by both the distal Asp and Arg residues (Fig. 2B), with a shorter H-bond length between the $N^{\eta1}$ atom of Arg342 and w1 (2.77 Å) compared

to 3.01 Å in DtpA. All other H-bonding interactions with Asp239 and Arg342 in DtpAa are mirrored in DtpA (Fig. 2B).

The distal w1 forms the base of an extended H-bonded H_2O network reaching upwards from the distal pocket (Fig. 2B); w1 is H-bonded to w2 (2.76 Å; B-factor 14.6 $Å^2$), w2 H-bonded to w3 (2.52 Å; B-factor 19.5 $Å^2$), w3 H-bonded to w4 (3.13 Å; B-factor 13.5 $Å^2$) and w4 H-bonded to w5 (2.81 Å; B-factor 10.1 $Å^2$). A similar H_2O network is found in the ferric DtpA structure (Fig. 2B), but it is notable that w3 and w4 occupy different spatial positions (Fig. 2B) and have a significantly shorter H-bonding distance of 2.81 Å, compared to 3.10 Å in DtpAa. In both DtpAa and DtpA, w5 is positioned at a surface opening, that has dimensions sufficient to enable H_2O_2 to enter, but not bulky organic substrates.

A second H-bonded H_2O channel leading from the distal side of the haem to the solvent exterior is present in ferric DtpAa (Fig. 2C). The N^{ε} atom of Arg342 H-bonds with w6 (2.77 Å; B-factor 12.8 $Å^2$), which is the start of a H-bonded H_2O chain that extends out perpendicular from the Arg342 side chain ending at w10 located at a second surface opening (Fig. 2C). Within this H_2O network, w8 participates in a H-bonding interaction with the $O^{\delta 2}$ atom (2.69 Å) of the haem propionate-7. Thus, both haem propionates participate in polar interactions that stem from the distal side of the haem. In ferric DtpA, an identical H-bonded H_2O channel is observed (Fig. 2C). Therefore, both the distal Arg and Asp residues are central components of two extensive H-bonding H_2O networks in both these ferric A-type DyPs.

The kinetics of Compound I formation in DtpAa

Rapid mixing of H_2O_2 with ferric DtpAa was carried out using a stopped-flow spectrophotometer operating in diode-array mode. Spectral transitions on mixing with H_2O_2 were observed that are consistent with the presence of an intermediate species, in going from the ferric species to Compound II. At pH 7.0, global analysis of the full spectral data using a sequential mechanism of $a \rightarrow b \rightarrow c$ (*i.e.* a = ferric, b = intermediate and c = Compound II) reveals the spectrum of the intermediate species, which possesses features consistent with a Compound I ([$(Fe^{4+}=O)$por•+]) species. Notably, the Soret band displays ~ 50 % decrease in absorbance together with a blue shift, with additional wavelength features in the red region of the spectrum that correlate with the Compound I spectrum of DtpA (Table 2, Fig. 3A and B). Fig 3A also depicts the kinetic traces at three wavelengths with their fits to the same model (*i.e.* $a \rightarrow b \rightarrow c$) and using the rate constants taken from the global fit (see Fig. 4). The residuals to the fits illustrate the model used for global analysis adequately describes both kinetic and

spectral data (inset Fig. 3A). Thus stopped-flow spectrophotometry confirms that Compound I is formed following addition of H_2O_2, but rapidly decays to Compound II. Pseudo-first order rate constants for ferric to Compound I (k_{obs1}) and Compound I to Compound II (k_{obs2}) were obtained from global fitting and are plotted as a function of increasing [H_2O_2] in Fig. 4A. For k_{obs1} a non-linear dependence on [H_2O_2] for Compound I formation is observed, with a steep increase in k_{obs1} values at low [H_2O_2], followed by a more gradual increase at higher [H_2O_2] (Fig. 4A). This behaviour is in stark contrast to DtpA, where a linear dependence on k_{obs1} with increasing [H_2O_2] between 12.5 and 75 μM is observed at pH 7.0 enabling a second-order rate constant of 8.9 x 10^6 M^{-1} s^{-1} to be determined.[27] The linear dependence of [H_2O_2] therefore indicates for DtpA that the binding of H_2O_2 to the ferric haem is rate limiting Compound I formation. For k_{obs2} little dependence on [H_2O_2] is observed (Fig. 4B), yielding a limiting rate constant for the decay of Compound I to Compound II of ~ 0.1 s^{-1}.

At pH 5.0 the global analysis of the full spectral data required a different model to account for the spectral transitions observed. The data now imply the existence of two ferric species reacting at different rates with H_2O_2 to form an intermediate and therefore a model of $a \rightarrow c$; $b \rightarrow c$; $c \rightarrow d$ (*i.e.* a = ferric^{I}, b = ferric^{II}, c = intermediate and d = Compound II) was used to yield the spectra shown in Fig. 3C and D. This kinetic model reveals that two ferric forms of DtpAa are present (ferric^{I} and ferric^{II} with a ratio of 50:60 *i.e.* ferric^{I} comprises 45% of the starting ferric DtpAa), with each form reacting with H_2O_2 at different rates to form a common intermediate assigned as Compound I, which then decays to Compound II (Fig. 3C and D). The inset to Fig. 3C shows a fit to the model $a \rightarrow c$; $b \rightarrow c$; $c \rightarrow d$ and to the simpler $a \rightarrow b \rightarrow c$ model (used at pH 7.0), with the accompanying residuals demonstrating that the model incorporating two ferric forms (blue line inset Fig. 3C) provides a more satisfactory description of the kinetics observed. Pseudo-first order rate constants for Compound I formation obtained from the global fitting are plotted against [H_2O_2] in Fig. 4B. The k_{obs1} values for the two ferric species reveal an initial dependence on H_2O_2 concentration, with ferric^{I} exhibiting similar k_{obs1} values to those determined at pH 7.0, whereas Compound I formation from ferric^{II} is ~ 2-times slower (Fig. 4B). At higher H_2O_2 concentrations both k_{obs1} values become rate limited. The decay of Compound I to Compound II again displays little H_2O_2 concentration dependence with a k_{obs2} value of ~ 0.15 s^{-1} determined (Fig. 4B). Overall these results appear to suggest that the kinetics of Compound I formation in DtpAa are rate limited at low [H_2O_2] by binding of H_2O_2 to the haem with a second rate limit being observed at higher [H_2O_2].

View Article Online
DOI: 10.1039/C9DT04583J

EPR characterisation of the ferric haem forms of DtpAa

The low-temperature (10 K) EPR spectra of ferric DtpAa (Fig. 5A), reveal features typical for a HS ferric haem in the g=6 region as well as at the g=2. It is clear that the HS spectrum at pH 5.0 comprises of two forms, while the spectrum at pH 7.0 only one of the forms is present (Fig. 5A), thus consistent with the findings from the stopped-flow experiments. Upon addition of 10-fold excess of H_2O_2 to DtpAa a series of samples were frozen at variable times and an EPR spectrum at each time point recorded (Fig. 5B). Spectral changes in the g=6 and g=2 regions were observed, but only the changes in the g=6 region associated with the ferric HS species are discussed further. The EPR spectra changes in the free radical region at g=2 were dramatic, and will be reported and discussed elsewhere. Analysis of the HS ferric haem spectra using spectra subtraction with variable coefficient procedure[49] enables the deconvolution of the HS ferric haem spectrum into two clear components, defined as HS_{narrow} and HS_{wide} (Fig. 5A and B). These two species are typical of many HS ferric haem (S=5/2) proteins and peroxidases, when the haem experiences a departure from the axial (tetragonal) symmetry and the principal g-values along two 'perpendicular' directions (in the haem plane) become unequal. The g-values of the HS ferric haem can be found from the second order spin Hamiltonian

$$\mathcal{H} = \beta \mathrm{gB\ S} + \mathrm{D}(S_z^2 - S(S+1)/3) + E(S_x^2 - S_y^2)$$

where B is external magnetic field, D describes a tetragonal component of the spin Hamiltonian, or axial zero field splitting component, and E, if present at all, introduces a rhombic component.[50] For most cases of non-zero rhombicity ($E \neq 0$), when E<<D, the principal g-values are well approximated as:

$$g_z = 6.00 - 24\ E/D,\ g_y = 6.00 + 24\ E/D,\ g_z = 2.00 - 34E^2/D^2$$

Thus, the zero field splitting rhombicity parameter E/D can be determined from the two g-values in the g=6 area:

$$E/D = (g_y - g_z)/48$$

The E/D parameter can take values from 0 for completely axial (tetragonal) haem to a theoretical maximal value of 1/3 for completely rhombic case.[51] In practice the E/D parameters for different haem proteins and enzymes (peroxidases and catalases) fit an approximate interval of 0 - 0.06.[52] The E/D values of the HS ferric haem forms detected in DtpAa, two at pH 5.0 and one at pH 7.0, are reported in Table 3, together with the g-values from which they have been calculated.

The two pure line shapes of the HS_{narrow} and HS_{wide} species were used to determine their respective contributions in each EPR spectrum associated with different reaction times

View Article Online
DOI: 10.1039/C9DT04583J

following addition of H_2O_2 (Fig. 5C). To express the HS_{narrow} and HS_{wide} signals intensities in terms of species concentration *i.e.* μM HS haem, the two signals were simulated (Fig. 5A and B) and the resulting line shapes double-integrated over the full range of magnetic field values of the signal (from 900 to 4600 G). This allows the kinetic curves plotted in Fig. 5C to be replotted in terms of HS haem species concentration (Fig. 5D). Fig. 5D supports the view that the HS_{narrow} and HS_{wide} species are both present and that H_2O_2 reacts with the HS_{narrow} form (less rhombic) rapidly, while the HS_{wide} form reacts in two phases to form Compound I; the majority at a rate comparable to that of the HS_{narrow} species and a minority species more slowly. At ~3 min, when all H_2O_2 is consumed, the ferric haem forms starts to recover, keeping the proportion of the HS_{narrow} and the HS_{wide} forms (the HS_{wide} form dominating). At 9 min, the proportion of the HS_{wide} and HS_{narrow} is very close to that observed in the control sample before H_2O_2 addition, *i.e.* HS_{wide} / HS_{narrow} ~ 4/3 *i.e.* HS_{narrow} comprising 43% of the starting ferric DtpAa.

The pH dependence of Compound I formation in DtpA and DtpAa

The pH dependence on the rate of Compound I formation for both DtpAa and DtpA on reacting with H_2O_2 was further explored (Fig. 6A and B). For DtpAa a bell-shaped pH profile is observed with k_{obs1} values increasing between pH values 4 and 7, followed by decreasing k_{obs1} values between pH 7 and 10. This behaviour indicates that two ionisation processes are detected with apparent pK_{a1} and pK_{a2} values of 4.87 ± 0.15 and 8.19 ± 0.16, respectively, determined from fitting the data in Fig 6A to a two proton ionisation equilibria equation. For DtpA the pH profile again reveals an increase in k_{obs1} values as the pH is increased from 4 to 6 leading to a plateau between pH 6 and 10 (Fig. 6B). A fit of the data in Fig. 6B to a single ionisation equilibrium equation yields an apparent pK_{a1} of 4.44 ± 0.15. Thus Compound I formation in both DtpA and DtpAa shares a common acidic ionisation equilibrium with a pK_a of ~ 4.5, which could possibly be assigned to an ionisable protein residue. In this respect both DtpAa and DtpA possess an Asp residue in the distal haem pocket, that has been strongly implicated in acting as an acid-base catalyst across the DyP sub-families. Alternatively, the possibility exists that we are monitoring the pK_a of the haem bound H_2O_2.

D_2O_2 as a mechanistic probe to study Compound I formation

To investigate further the mechanism of Compound I formation, H_2O_2 was substituted with D_2O_2. As Compound I formation is associated with the breakage and formation of an O-H

bond, then using D_2O_2 will reveal if these steps are rate limiting. For these experiments both peroxidases were exchanged into a D_2O buffer (*i.e.* the solvent used) and therefore a kinetic isotope effect (KIE) instead of a solvent KIE (sKIE) is used to describe Compound I formation. At pD 7.0 a linear dependence of k_{obs1} on increasing [D_2O_2] was observed with DtpA enabling a second-order rate constant (k_D) of 1.1 ± 0.5 x 10^7 $M^{-1}s^{-1}$ for Compound I formation to be determined (Fig. 7A), which is identical within error to the value determined in H_2O (k_H = 8.9 ± 0.3 x 10^6 $M^{-1}s^{-1}$).[27] Thus, for DtpA the k_H/k_D = 0.8 (*i.e.* < 1) indicating no KIE. For DtpAa a similar kinetic profile with D_2O_2 as with H_2O_2 is observed (Fig. 7B), but now the k_{obs1} values decrease with an average k_{obs1H}/k_{obs1D} = 1.8 indicating a KIE for DtpAa (Fig. 7B). For k_{obs2} (decay of Compound I to Compound II) a limiting rate constant with D_2O_2 is observed as with H_2O_2 with the average k_{obs2H}/k_{obs2D} = 0.9 meaning no KIE (Fig. 7C). Together, these results confirm that for DtpAa the rate determining step for Compound I formation is proton-transfer, following binding of H_2O_2 to the ferric haem, whereas for DtpA the absence of a KIE suggests that proton-transfer is faster than H_2O_2 binding.

Removal of the distal Asp in DtpAa and DtpA decreases the rate of Compound I formation

To address the role of the distal Asp in the mechanism of Compound I formation, the D251A and D239A variants of DtpA and DtpAa, respectively, were prepared. The absorbance spectra of the two variants are shown in Fig. S2 with wavelength maxima reported in Table 2. Addition of one-equivalent of H_2O_2 to the ferric form of either variant results in the appearance of a spectrum consistent with a Compound II species (Fig. S2 and Table 2). Thus, in contrast with wild-type DtpA in which a Compound I spectrum forms and slowly decays back to the ferric form,[27] the removal of the distal Asp may suggest destabilisation of Compound I.

The kinetics of Compound I formation for the distal Asp variants was monitored using a stopped-flow spectrophotometer operating in diode-array mode. Spectral transitions on mixing with H_2O_2 were consistent with the presence of an intermediate species assigned as Compound I before decaying to Compound II (Fig. S2). It is notable that for both Asp variants the k_{obs1} values are on the order of a few per second and therefore comparable to wild-type DtpAa. At pH 5.0 the D251A variant displays a linear dependence of k_{obs1} values with [H_2O_2] yielding a second-order rate constant of 4.27 ± 0.07 x 10^3 M^{-1} s^{-1}, 4-orders of magnitude slower than wild-type DtpA and thus providing a clear indication that the distal Asp in DtpA accelerates the reaction with H_2O_2. For k_{obs2} little dependence on [H_2O_2] is observed (Fig. 8B), yielding a limiting rate constant for the decay of Compound I to Compound II of ~ 0.08 s^{-1}, a

kinetic parameter not possible to determine directly for wild-type DtpA, but maybe inferred to be ~ 0.005 s^{-1} by using a previously reported value of $t_{1/2}$ = 2.5 min for the decay of Compound I to the form the ferric species in a mechanism in which intermediate Compound II is populated at a low level.[27] In both the wild-type DtpA and the D251A variant, the rate of Compound I formation is greater than the rate of its decay (DtpA with 50 μM H_2O_2 k_{obs1}/k_{obs2} = 5 x 10^4 and for the D251A variant 500 μM H_2O_2 k_{obs1}/k_{obs2} = 25). The maximal fraction of the total protein appearing as the intermediate Compound I, $[CmpdI]_{max}$, may be calculated from

$$[CmpdI]_{max} = \left(\frac{k_{obs2}}{k_{obs1}}\right)^{\left(\frac{k_{obs2}}{k_{obs1} - k_{obs2}}\right)}$$

Therefore, for DtpA, the k_{obs1}/k_{obs2} ratio shows that Compound I is essentially maximally formed, *i.e.* 100% of the enzyme is in this form prior to decay, while for the D251A variant the k_{obs1}/k_{obs2} shows that Compound I maximally comprises 88% of the enzyme. Thus in both enzymes, Compound I is essentially fully formed and thereafter decays, in the D251A variant 16-fold faster than in the wild-type DtpA, consistent with our suggestion that removal of the distal Asp residue destabilises Compound I in the D251A variant.

At pH 7.0, the k_{obs1} values for the D251A variant become rate limited at high $[H_2O_2]$, and substitution with D_2O_2 gives an average k_{obs1H}/k_{obs1D} = 2.0 indicating a KIE (inset Fig. 8A). The pH dependence of Compound I formation for the D251A variant is shown in Fig. 8C, and notably displays two ionisation equilibria with pK_{a1} = 5.10 ± 0.21 and pK_{a2} = 8.02 ± 0.50. Thus in the absence of the distal Asp an acidic ionisation equilibrium remains with a pK_a comparable to that of wild-type DtpA, and a second ionisation equilibrium is apparent that was not present in the wild-type enzyme.

For the D239A variant of DtpAa, the kinetics of Compound I formation could be followed at pH 5.0 but not at pH 7.0 owing to the rapid decay of Compound I to Compound II resulting in no clear assignment of an intermediate with Compound I spectral features. Therefore, a complete pH profile for Compound I formation could not be determined for the D239A DtpAa variant. However, for pH values between 5.0 and 6.0, where Compound I could be detected, k_{obs1} values show an increase as noted in DtpA, DtpAa and the D251A variant. At pH 5.0 the k_{obs1} value are of a similar order to wild-type DtpAa and the kinetic profile is strongly comparable to the wild-type enzyme (Fig. 8D). Thus in DtpAa removal of the Asp is of little consequence to Compound I formation.

DISCUSSION

Haem peroxidases are typically crystallised in the ferric resting state, but are extremely susceptible to X-ray driven reduction during crystallographic data collection. As commented on previously,[28] amongst the > 50 deposited structural coordinates of DyP members in the PDB, there is a dearth of supporting information regarding the haem oxidation state for these depositions. The absence of this information does not therefore allow for confident comparison of haem pocket structures to be made within the DyP sub-families and makes structure guided mechanistic insights problematic. As part of the present work the cryo-cooled X-ray structure of DtpAa has been unambiguously determined to be in the ferric haem oxidation state, thus enabling comparison with the cryo-cooled ferric DtpA structure[28] and also the room temperature XFEL structure of ferric DtpAa.[30] Whilst, the major aim for the present work is an investigation of mechanistic differences between two A-type DyP homologues, it is worth briefly comparing the haem pockets between the room temperature and cryo-cooled DtpAa ferric structures. In both DtpAa structures the bond-length for the haem bound distal H_2O molecule is significantly longer than in the ferric DtpA structure (Fig. 2). Notably, the side chain position of the distal Asp in both DtpAa structures is identical, but differs from DtpA where the side chain $O^{\delta 1/2}$ atoms are further away from the distal haem face and do not participate in a H-bond interaction with the haem bound distal H_2O molecule, which is the case in ferric DtpAa (Fig. 2). We believe this subtle change in side chain position has significant consequences for H_2O_2 reactivity and will be discussed further. Both DtpAa structures have an extensive network of distal H-bonded H_2O networks arranged around the Asp-Arg couple, which are superimposable and we therefore conclude that no temperature dependent haem pocket changes in the ferric DtpAa structures are apparent.

A mechanism which can provide a consistent picture of Compound I formation in DtpAa and DtpA is depicted in Figure 9. The mechanism comprises six steps. Step 1 is the dissociation of the distal H_2O molecule from the ferric haem, step 2 is the second order binding of peroxide to the ferric haem to form the neutral Compound 0 complex (Fe^{III}-OH^{α}–OH^{β}), step 3 is the dissociation of the H^{α} proton to form the anionic Compound 0 complex (Fe^{III}-O^{α}–OH^{β}), step 4 is the association of the H^{α} proton with the distal Asp, step 5 comprises the movement of the H^{α} proton from the Asp to the OH^{β} and step 6 is the heterolysis of the O-O bond and electron transfer to form Compound I. Within the framework of the structural, kinetic and thermodynamic results presented above, the mechanism depicted in Fig. 9 forms the basis for the following discussion on the different kinetic behaviours observed for DtpA and DtpAa upon reaction with H_2O_2.

By validating the ferric X-ray structures of both DtpAa and DtpA, the requirement for step 1 in our mechanism is accounted for. Both enzymes display an extensive network of H-bonded H_2O molecules that communicate with the distal Asp-Arg couple (Fig. 2). For H_2O_2 to bind (step 2) the distal haem bound H_2O must be displaced. In DtpA the linear dependence of the rate of Compound I formation on $[H_2O_2]$ is an indication that the rate determining step in our mechanism of Compound I formation is the binding of H_2O_2 to the ferric haem (step 2). As binding of H_2O_2 to DtpA is rapid, this indicates that the ferric haem site is labile, *i.e.* the H_2O dissociation (step 1) does not impede the binding of H_2O_2 (step 2). Were the preceding H_2O dissociation step to be rate limiting, there would be no linear dependency of the rate constant on H_2O_2 concentration. Replacement of H_2O_2 with D_2O_2 revealed no KIE and thus indicates that proton-transfer (steps 4 and 5) is much faster than H_2O_2 binding (step 2). Furthermore, our data show that the rate of Compound I formation in both DtpA and DtpAa is pH dependent. Both enzymes share an ionisation equilibrium with an apparent pK_a of ~4.5. Notably, an acidic ionisation process is also observed in the distal Asp variant of DtpA (and can be inferred for the distal Asp variant of DtpAa), suggesting that the observed pK_a cannot be attributed to the distal Asp. In this respect it has been reported that binding of H_2O_2 to the ferric haem in peroxidases to form the Fe^{III}-OH^{α}–OH^{β} complex, promotes the ionisation of H_2O_2 by decreasing the pK_a of the free H_2O_2 from ~11.5 to ~5.5 in the haem bound state.[16, 18] Such a decrease in the pK_a is consistent with a simple calculation of $\Delta G_{el} = 1347(q_1q_2)/\varepsilon D$, where ΔG_{el} is the electrostatic interaction free energy (kJ/mol at 298 K), q_1 and q_2 are the charges on the iron porphyrin and the proton (unity in both cases), ε is the appropriate dielectric constants and D is distance of the charges in Å (we have used a value of 2 Å).[53] Moore suggests a reasonable value for εD is approximately 40.[54] Given this, we calculate ΔG_{el} of the order 34 kJ/mol, which equates to a change in pK_a of 6 pH units. Thus a decrease in the pK_a of H_2O_2 from 11.5 to 5.5 on binding to the haem is consistent with theoretical calculations. Therefore, we attribute the acidic pK_a observed in the present studies to the deprotonation/protonation of the H_2O_2 bound to the haem, which is common to all the enzymes studied. Incidentally, two recent studies with B-type DyPs have indicated that the pK_a of the distal Asp is << 4,[25, 26] and therefore in our mechanism we depict the Asp as being in an anionic state (Fig. 9). However, to account for our experimental observations, that an acidic ionisation process occurs for both A-type DyPs with and without the distal Asp residue, we propose in our mechanism that the H^{α} proton of the Fe^{III}-OH^{α}–OH^{β} complex deprotonates to first form a hydronium ion (step 3). Subsequently, in the case of DtpA, the H^{α} proton is then transferred from the hydronium ion onto the distal Asp

transiently (step 4), followed by transfer to the OH^{β} (step 5) prior to heterolysis of the O-O bond. As noted by the absence of a KIE, these proton-transfer steps in DtpA are highly optimised and are faster than the initial H_2O_2 binding.

For the D251A variant of DtpA, the linear dependence on the rate of Compound I formation at pH 5.0 with $[H_2O_2]$ (Fig. 8A) is a further indication that the rate determining step is the binding of H_2O_2 to the ferric haem (step 2). The second-order rate constant is now 2000-fold lower than for wild-type DtpA, suggesting that the distal Asp is important for facilitating favourable H_2O_2 binding to form the initial Fe^{III}-OH^{α}–OH^{β} complex (step 2). The slightly elevated pK_a for the H^{α} in the Fe^{III}-OH^{α}–OH^{β} complex in the absence of the Asp, as compared to the wild-type enzyme (5.10 *vs* 4.44, respectively), serves to illustrate that the distal Asp also tunes the ionisation properties of the haem bound H_2O_2. At pH 5.0, proton-transfer in the D251A variant remains efficient *i.e.* faster than H_2O_2 binding, despite the absence of the Asp. We note that in DtpA and DtpAa, two extensive networks of H-bonded H_2O molecules that communicate with the Asp and the Arg residue are a dominating feature of the distal pocket (Fig. 2B and C). In other peroxidases such as APX or CcP,[55, 56] the distal pocket H_2O network is notably less extensive. It is well documented that H_2O networks in proteins can facilitate proton transfer.[57] Recent insights into the contribution of H_2O networks to proton movement/transfer have highlighted the importance of the directionality of the H-bonded H_2O network, *i.e.* chains of H_2O molecules linked in donor-acceptor configurations that are highly favoured for proton-transfer.[58] In the absence of the Asp and w2, we suggest for the D251A variant steps 4 and 5 in our mechanism still occur but the 'substitute' for w2 in the variant is not optimally configured for proton-transfer from the hydronium ion to the OH^{β}, but nevertheless is faster than H_2O_2 binding at pH 5.0 (step 2). At pH 7.0, the k_{obs1} for Compound I formation in the D251A variant approaches a rate limit, which we now assign to proton-transfer becoming rate limiting, confirmed by substitution with D_2O_2. Thus in the D251A variant, whether H_2O_2 binding or proton-transfer is rate limiting is finely balanced and this balance can be perturbed through changes in pH or substitution by D_2O_2.

For DtpAa, the kinetics observed are considerably different from those for DtpA. Compound I formation in DtpAa appears to be initially $[H_2O_2]$ dependent, indicating that step 2 in our mechanism is rate limiting. However, as $[H_2O_2]$ increases, the rate limit transfers to step 4 and 5 (*i.e.* proton-transfer), which is corroborated upon substituting H_2O_2 with D_2O_2 (Fig. 7B). Thus, for DtpAa as noted for the D251A DtpA variant, there appears to be a fine balance in the kinetic phases that distinguish the events determining the rate limiting steps in

the mechanism of Compound I formation. Furthermore, the dependence of k_{obs1} values at low $[H_2O_2]$, when H_2O_2 binding may be considered as being rate limiting for DtpAa, are now a few per second, ~100-fold lower than for DtpA, leading to the conclusion that DtpAa is a poor peroxidase. In fact the k_{obs1} values for DtpAa are comparable with the D251A variant of DtpA and the D239A variant of DtpAa, revealing that even when the distal Asp is present, the rate of Compound I formation is clearly suppressed compared to DtpA. Why might this be? The structural data reveal a subtle positional change of the distal Asp side chain in DtpAa, whereby it encroaches towards the distal haem face enabling a H-bond interaction between the haem bound H_2O molecule and the $O^{\delta 1}$ atom of the Asp (Fig. 2). Now, the haem bound H_2O molecule in DtpAa has an additional interaction compared to DtpA, where despite the shorter Fe(III)-OH_2 bond length, the absence of an additional constraint imposed directly by the distal Asp makes an argument for a more labile haem bound H_2O in DtpA. Therefore, at low $[H_2O_2]$, when H_2O_2 binding may be considered as being rate limiting for DtpAa, the much decreased k_{obs1} values compared to DtpA, could arise as a consequence of a decreased lability of the distal haem bound H_2O in DtpAa, resulting in the rate being limited by the H_2O dissociation (step 1). However, as noted, low k_{obs1} values are also observed for both Asp variants, where although no structural information is available to inform whether a haem bound water is present, the absence of the Asp, makes the lability of the H_2O argument less compelling. A further possibility to consider is that the repositioning of the Asp in DtpAa imposes steric constraints, that could lead to hindering the rate of H_2O_2 binding and its stabilisation in the Fe^{III}-OH^{α}–OH^{β} complex and decrease the efficiency of (rapid) proton-transfer (steps 4 and 5) through the Asp side chain not being optimally orientated to ensure such transfer. We note the binding of H_2O_2 to the ferric haem is decreased in the H42L variant of HRP, which has been explained through steric impediment of the Leu side chain and importantly for the stringent requirement of H-bonding between the distal His42 and the Fe^{III}-OH^{α}–OH^{β} complex.[18] Thus we suggest that the Asp in DtpAa impedes optimal stabilisation of the Fe^{III}-OH^{α}–OH^{β} complex and optimal proton-transfer (steps 4 and 5), whereas in DtpA the Asp position is optimised for rapid H_2O_2 binding and proton-transfer. The similarity of rates with the Asp variants support this proposal. Therefore, the slight structural movement of the Asp in DtpAa tips the balance between rate limiting steps from H_2O_2 binding to proton-transfer.

Comparison of the pH dependencies of k_{obs1} for DtpA, DtpAa and the D251A variant of DtpA, reveal significant differences above pH 7.0. For DtpA, the rate constant is pH independent above pH 7.0 indicating that the rate limit remains H_2O_2 binding and proton

transfer is rapid and efficient, suggesting that the finely tuned structure within the haem pocket that delivers the proton for O-O scission remains intact. In the case of DtpAa, in which as discussed the Asp is not optimally positioned for proton-transfer, above pH 7.0 a second ionisation equilibrium with a pK_a of 8.19 is observed. Similarly, the DtpA D251A variant displays a second ionisation equilibrium with a pK_a of 8.0, which is not the case for the wild-type DtpA. Both DtpAa and the DtpA D251A variant exhibit a KIE showing that proton-transfer is rate limiting and thus the distal pocket is not tuned as it is in DtpA. Thus, where a KIE is seen, we also observe an ionisation process above pH 7.0. We suggest this may arise from an ionisable group that competes for the hydronium ion proton and thus decreases the fraction of the enzyme entering the productive route to Compound I. In DtpA this postulated group is unable to compete in this manner because of the finely tuned architecture of the pocket as discussed above.

Finally, we comment briefly on the two forms of DtpAa observed by EPR and optical spectra collected in stopped-flow experiments at pH 5.0. The two forms, ferric^{I} and ferric^{II} have distinct properties, with ferric^{I} having the narrower splitting of the two g-perpendicular components of the HS g=6 signal, resulting in E/D = 0.005, a value close to cytochrome *c* oxidase and the other form, ferric^{II} has a E/D = 0.015 which is similar to HRP.[52] While rhombicity of HS_{wide} is ~3 time greater than of HS_{narrow}, both forms fit well the previously reported range of E/D in haem proteins.[52] In a recent study with a genetically engineered myoglobin, a clear correlation is drawn between the ligand arrangement in the distal site of the haem, seen in the crystal structure, and the rhombicity detectable in the EPR spectra, with the E/D value changing from 0.002 to 0.042.[59] Therefore, in simple terms the EPR of DtpAa may be accounted for by proposing that a haem pocket acid group is deprotonated at pH 7.0 (only one form) and at pH 5.0 exists in approximately 50 % deprotonated/protonated forms. The negative charge on this deprotonated acid group perturbs the electronic structure of the haem iron rendering this asymmetry of the otherwise axial g-tensor at pH 7.0. A combination of two electronic structures with different degrees of rhombicity (departure from the axial) at pH 5.0, result from the co-existence of the charged and neutral species. The more rhombic form (seen at pH 7.0 and termed ferric^{II} at pH 5.0) has the HS_{wide} spectrum, while ferric^{I} seen at pH 5.0 is the more axial HS_{narrow} spectrum. Moreover, our stopped-flow experiments indicate ferric^{I} reacts more rapidly with H_2O_2, while ferric^{II} reacts more slowly with H_2O_2. Although this cannot be seen directly in the EPR experiments, because the appropriate time range is not accessible (*i.e.* within 2 seconds), EPR do reveal that there are kinetic differences between ferric^{I} and ferric^{II} in a longer time range (Fig. 5). Our present work does not enable the nature

View Article Online
DOI: 10.1039/C9DT04583J

of the group to be identified and further studies are required to elucidate this, together with the mechanism through which we may connect the EPR spectrum with the observed kinetics.

SUMMARY

In conclusion we have shown that a common mechanism for Compound I formation in two A-type DyPs is influenced by a subtle structural change in the distal haem pocket, which affects the steric approach of H_2O_2 and the way protons are moved in the haem pocket. Remarkably, this difference would appear to account for DtpA reacting rapidly and efficiently with H_2O_2 as opposed to the extremely poor reactivity for DtpAa. Furthermore, the study of these enzymes has allowed us to propose that the pH dependency observed in the acid region is determined not by an ionisable protein residue(s) but by the pK_a of the haem bound peroxide. From a functional perspective our findings serve to advance the notion that not all DyP members possess efficient peroxidase reactivity despite the fold and architecture of the haem pocket being similar. As a corollary to this notion, DtpA will therefore be the dominant sensor of H_2O_2 in *S. lividans*, whereas a function, other than as a peroxidase for DtpAa, awaits elucidation.

ACKNOWLEDGEMENTS

M.L. is the recipient of a Peter Nicholls Scholarship and A.K.C. the recipient of a Silberrad Scholarship. M.A.H. acknowledges funding from The Leverhulme Trust (RPG-2014-355) and the Swiss Light Source Long Term beamtime award 20160704.

CONFLICT OF INTEREST

The authors declare no conflicts of interest.

REFERENCES

1. X. Huang and J. T. Groves, *Chemical reviews*, 2018, **118**, 2491-2553.
2. H. B. Dunford, *Peroxidases and Catalases: Biochemistry, Biophysics, Biotechnology, and Physiology*, Wiley, 2nd edn., 2010.
3. T. L. Poulos, *Chem Rev*, 2014, **114**, 3919-3962.
4. D. Dolphin, A. Forman, D. C. Borg, J. Fajer and R. H. Felton, *Proc Nat Acad Sci USA*, 1971, **68**, 614-618.
5. A. N. Hiner, E. L. Raven, R. N. Thorneley, F. Garcia-Canovas and J. N. Rodriguez-Lopez, *J Inorg Biochem*, 2002, **91**, 27-34.
6. P. C. E. Moody and E. L. Raven, *Accounts of chemical research*, 2018, **51**, 427-435.
7. S. J. Kim and M. Shoda, *Appl Environ Microbiol*, 1999, **65**, 1029-1035.
8. R. Singh and L. D. Eltis, *Arch Biochem Biophys*, 2015, **574**, 56-65.
9. K. Sugawara, E. Igeta, Y. Amano, M. Hyuga and Y. Sugano, *AMB Express*, 2019, **9**, 56.

10. N. Fawal, Q. Li, B. Savelli, M. Brette, G. Passaia, M. Fabre, C. Mathe and C. Dunand, *Nucleic Acids Res*, 2013, **41**, D441-444.
11. T. Yoshida and Y. Sugano, *Arch Biochem Biophys*, 2015, **574**, 49-55.
12. M. H. Habib, H. J. Rozeboom and M. W. Fraaije, *Molecules*, 2019, **24**.
13. T. L. Poulos, S. T. Freer, R. A. Alden, S. L. Edwards, U. Skogland, K. Takio, B. Eriksson, N. Xuong, T. Yonetani and J. Kraut, *J Biol Chem*, 1980, **255**, 575-580.
14. M. Gajhede, D. J. Schuller, A. Henriksen, A. T. Smith and T. L. Poulos, *Nat Struct Biol*, 1997, **4**, 1032-1038.
15. Y. Sugano, R. Muramatsu, A. Ichiyanagi, T. Sato and M. Shoda, *J Biol Chem*, 2007, **282**, 36652-36658.
16. J. E. Erman, L. B. Vitello, M. A. Miller, A. Shaw, K. A. Brown and J. Kraut, *Biochemistry*, 1993, **32**, 9798-9806.
17. B. D. Howes, J. N. Rodriguez-Lopez, A. T. Smith and G. Smulevich, *Biochemistry*, 1997, **36**, 1532-1543.
18. J. N. Rodriguez-Lopez, D. J. Lowe, J. Hernandez-Ruiz, A. N. Hiner, F. Garcia-Canovas and R. N. Thorneley, *J Am Chem Soc*, 2001, **123**, 11838-11847.
19. T. L. Poulos and J. Kraut, *J Biol Chem*, 1980, **255**, 8199-8205.
20. P. Vidossich, G. Fiorin, M. Alfonso-Prieto, E. Derat, S. Shaik and C. Rovira, *J Phys Chem B*, 2010, **114**, 5161-5169.
21. H. K. Baek and H. E. Van Wart, *Biochemistry*, 1989, **28**, 5714-5719.
22. D. A. Svistunenko, B. J. Reeder, M. M. Wankasi, R. L. Silaghi-Dumitrescu, C. E. Cooper, S. Rinaldo, F. Cutruzzola and M. T. Wilson, *Dalton Trans*, 2007, **8,** 840-850.
23. R. Singh, J. C. Grigg, Z. Armstrong, M. E. Murphy and L. D. Eltis, *J Biol Chem*, 2012, **287**, 10623-10630.
24. S. Mendes, V. Brissos, A. Gabriel, T. Catarino, D. L. Turner, S. Todorovic and L. O. Martins, *Arch Biochem Biophys*, 2015, **574**, 99-107.
25. R. Shrestha, G. C. Huang, D. A. Meekins, B. V. Geisbrecht and P. Li, *ACS Cat*, 2017, **7**, 6352-6364.
26. V. Pfanzagl, K. Nys, M. Bellei, H. Michlits, G. Mlynek, G. Battistuzzi, K. Djinovic-Carugo, S. Van Doorslaer, P. G. Furtmuller, S. Hofbauer and C. Obinger, *J Biol Chem*, 2018, **293**, 14823-14838.
27. A. K. Chaplin, M. T. Wilson and J. A. R. Worrall, *Dalton Trans*, 2017, **46**, 9420-9429.
28. A. K. Chaplin, T. M. Chicano, B. V. Hampshire, M. T. Wilson, M. A. Hough, D. A. Svistunenko and J. A. R. Worrall, *Chemistry*, 2019, **25**, 6141-6153.
29. M. L. Petrus, E. Vijgenboom, A. K. Chaplin, J. A. Worrall, G. P. van Wezel and D. Claessen, *Open Biol*, 2016, **6**.
30. A. Ebrahim, T. Moreno-Chicano, M. V. Appleby, A. K. Chaplin, J. H. Beale, D. A. Sherrell, H. M. E. Duyvesteyn, S. Owada, K. Tono, H. Sugimoto, R. W. Strange, J. A. R. Worrall, D. Axford, R. L. Owen and M. A. Hough, *IUCrJ*, 2019, **6**, 543-551.
31. I. Schlichting, *Acc Chem Res*, 2000, **33**, 532-538.
32. G. I. Berglund, G. H. Carlsson, A. T. Smith, H. Szoke, A. Henriksen and J. Hajdu, *Nature*, 2002, **417**, 463-468.
33. A. Gumiero, C. L. Metcalfe, A. R. Pearson, E. L. Raven and P. C. Moody, *J Biol Chem*, 2011, **286**, 1260-1268.
34. C. M. Casadei, A. Gumiero, C. L. Metcalfe, E. J. Murphy, J. Basran, M. G. Concilio, S. C. Teixeira, T. E. Schrader, A. J. Fielding, A. Ostermann, M. P. Blakeley, E. L. Raven and P. C. Moody, *Science*, 2014, **345**, 193-197.

35. G. Chreifi, E. L. Baxter, T. Doukov, A. E. Cohen, S. E. McPhillips, J. Song, Y. T. Meharenna, S. M. Soltis and T. L. Poulos, *Proc Nat Acad Sci U S A*, 2016, **113**, 1226-1231.
36. H. Kwon, J. Basran, C. M. Casadei, A. J. Fielding, T. E. Schrader, A. Ostermann, J. M. Devos, P. Aller, M. P. Blakeley, P. C. Moody and E. L. Raven, *Nat Commun* 2016, **7**, 13445.
37. H. Kwon, O. Smith, E. L. Raven and P. C. Moody, *Acta Crystallogr D*, 2017, **73**, 141-147.
38. R. F. Beers, Jr. and I. W. Sizer, *J Biol Chem*, 1952, **195**, 133-140.
39. D. A. Svistunenko, N. Davies, D. Brealey, M. Singer and C. E. Cooper, *Biochim Biophys Acta*, 2006, **1757**, 262-272.
40. M. R. Fuchs, C. Pradervand, V. Thominet, R. Schneider, E. Panepucci, M. Grunder, J. Gabadinho, F. S. Dworkowski, T. Tomizaki, J. Schneider, A. Mayer, A. Curtin, V. Olieric, U. Frommherz, G. Kotrle, J. Welte, X. Wang, S. Maag, C. Schulze-Briese and M. Wang, *J Synchrotron Radiat*, 2014, **21**, 340-351.
41. W. Kabsch, *Acta Crystallogr D,* 2010, **66**, 125-132.
42. G. N. Murshudov, A. A. Vagin and E. J. Dodson, *Acta Crystallogr D,* 1997, **53**, 240-255.
43. D. Liebschner, P. V. Afonine, M. L. Baker, G. Bunkoczi, V. B. Chen, T. I. Croll, B. Hintze, L. W. Hung, S. Jain, A. J. McCoy, N. W. Moriarty, R. D. Oeffner, B. K. Poon, M. G. Prisant, R. J. Read, J. S. Richardson, D. C. Richardson, M. D. Sammito, O. V. Sobolev, D. H. Stockwell, T. C. Terwilliger, A. G. Urzhumtsev, L. L. Videau, C. J. Williams and P. D. Adams, *Acta Crystallogr D,* 2019, **75**, 861-877.
44. P. Emsley, B. Lohkamp, W. G. Scott and K. Cowtan, *Acta Crystallogr* 2010, **66**, 486-501.
45. I. W. Davis, A. Leaver-Fay, V. B. Chen, J. N. Block, G. J. Kapral, X. Wang, L. W. Murray, W. B. Arendall, 3rd, J. Snoeyink, J. S. Richardson and D. C. Richardson, *Nucleic Acids Res*, 2007, **35**, W375-383.
46. O. B. Zeldin, M. Gerstel and E. F. Garman, *J Appl Crystallogr*, 2013, **46**, 1225-1230.
47. K. S. D. Kumar, M. Gurusaran, S. N. Satheesh, P. Radha, S. Pavithra, K. P. S. T. Tharshan, J. R. Helliwell and K. Sekar, *J Appl Crystallogr*, 2015, **48**, 939-942.
48. M. Gurusaran, M. Shankar, R. Nagarajan, J. R. Helliwell and K. Sekar, *IUCrJ*, 2014, **1**, 74-81.
49. D. A. Svistunenko, N. Davies, D. Brealey, M. Singer and C. E. Cooper, *Biochim Biophys Acta*, 2006, **1757**, 262-272.
50. C. P. Scholes, *Proc Nat Acad Sci U S A*, 1969, **62**, 428-431.
51. W. E. Blumberg, J. Peisach, B. A. Wittenberg and J. B. Wittenberg, *J Biol Chem*, 1968, **243**, 1854-1862.
52. J. Peisach, W. E. Blumberg, S. Ogawa, E. A. Rachmilewitz and R. Oltzik, *The J Biol Chem*, 1971, **246**, 3342-3355.
53. C. E. Schulz and R. H. Schirmer, *Principles of Protein Structure* Springer-Verlag, Berlin, New York, 1979.
54. G. R. Moore, *FEBS Letts*, 1983, **161**, 171-175.
55. C. A. Bonagura, B. Bhaskar, H. Shimizu, H. Li, M. Sundaramoorthy, D. E. McRee, D. B. Goodin and T. L. Poulos, *Biochemistry*, 2003, **42**, 5600-5608.
56. K. H. Sharp, M. Mewies, P. C. Moody and E. L. Raven, *Nat Struct Biol*, 2003, **10**, 303-307.
57. H. Ishikita and K. Saito, *J Roy Soc Inter*, 2014, **11**.
58. A. Hassanali, F. Giberti, J. Cuny, T. D. Kuhne and M. Parrinello, *Proc Nat Acad Sci U S A*, 2013, **110**, 13723-13728.

59. S. Chand, S. Ray, E. Wanigasekara, P. Yadav, J. A. Crawford, D. W. Armstrong, K. Rajeshwar and B. S. Pierce, *Arch Biochem Biophys*, 2018, **639**, 44-51.

View Article Online
DOI: 10.1039/C9DT04583J

Table 1: X-ray crystallography data processing and refinement statistics for ferric DtpAa. Values in parenthesis refer to the outermost resolution shell.

Space group	$P2_1$
Unit cell (Å)	a=71.4, b=67.59, c= 72.9, β = 105.5°
Resolution (Å)	48.71 - 1.80
Outer shell (Å)	1.84 - 1.80
Unique reflections	61725 (3542)
Mn (I/SD)	6.3 (1.6)
$CC_{1/2}$	0.989 (0.683)
Completeness (%)	99.4 (96.1)
Redundancy	4.5 (2.9)
R_{cryst}	0.1513
R_{free}	0.1991
RMS dev. bond lengths (Å)	0.009
RMS dev. bond angles (°)	1.000
Ramachandran favoured (%)	98.19
PDB accession code	6TB8

Table 2: Wavelength absorbance maxima at pH 7.0 for DtpAa and DtpA and the respective distal Asp variants.

Protein	Ferric (nm)	Compound I (nm)	Compound II (nm)
DtpAa	406, 500, 540 (sh)[a], ~ 588, 630	[c]403, 534, 588, 614, 641	416, 527, 557, 620
DtpA[b]	406, 502, 540 (sh), 635	399, 530, 557, 614, 644	419, 528, 557, 621
D239A DtpAa	410, 504, 569, 636, 687	n.d.	418, 528, 556, 632,686
D251A DtpA	408, 501, 542 (sh), ~ 589, 635	[c]400, 539, 588, 605, 638	418, 528, 558, 615, 638

[a]Shoulder (sh)
[b]Values taken from [27].
[c]Values taken from global fitting of the spectral transitions observed upon mixing with H_2O_2 in stopped-flow spectrophotometer.

Table 3. The principal g-values, rhombicity parameters E/D, individual line widths and Lorentz/Gaussian line shape ratios used in the simulation of the EPR signals of the two HS ferric haem forms of DtpAa.

	g_1	g_2	g_3	E/D	ΔH_1, G	ΔH_2, G	ΔH_3, G	Lorentz/Gaussian ratio
HS_{narrow}	6.025	5.804	1.999	0.0046	15	15	15	0.1
HS_{wide}	6.220	5.510	1.992	0.0148	20	20	20	0.1
$HS_{wide, pH7}$	6.210	5.505	1.992	0.0147	23	25	25	0.1

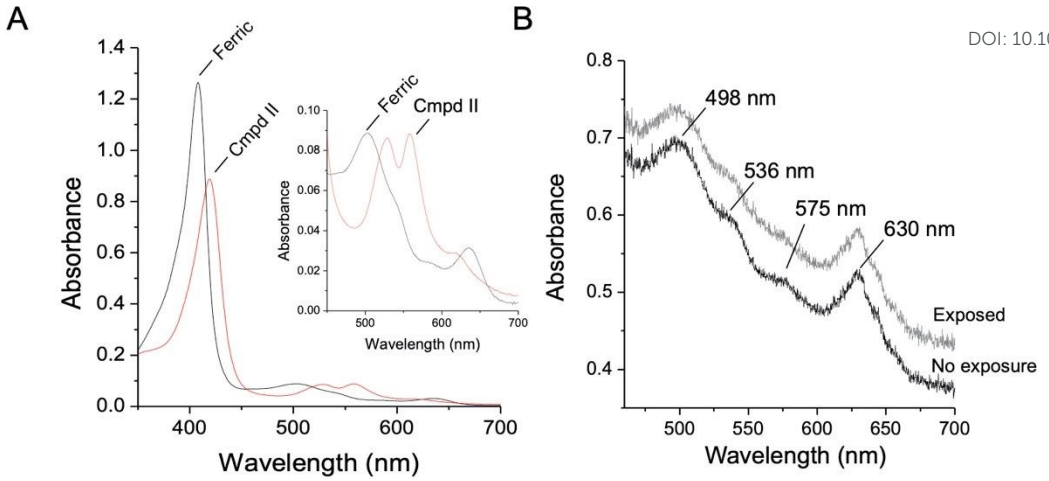

Figure 1: Electronic absorbance spectra of DtpAa. A) Solution spectra at pH 7.0 with the ferric and Compound II (Cmpd II) species, the latter formed following addition of one molar equivalent of H_2O_2 per molar haem, indicated. *Inset* a zoom-in of the α/β band region. B) The α/β band region of a crystal of ferric DtpAa recorded at 100 K before (no X-ray exposure) and after exposure to X-rays following collection of a 20° data wedge.

View Article Online
DOI: 10.1039/C9DT04583J

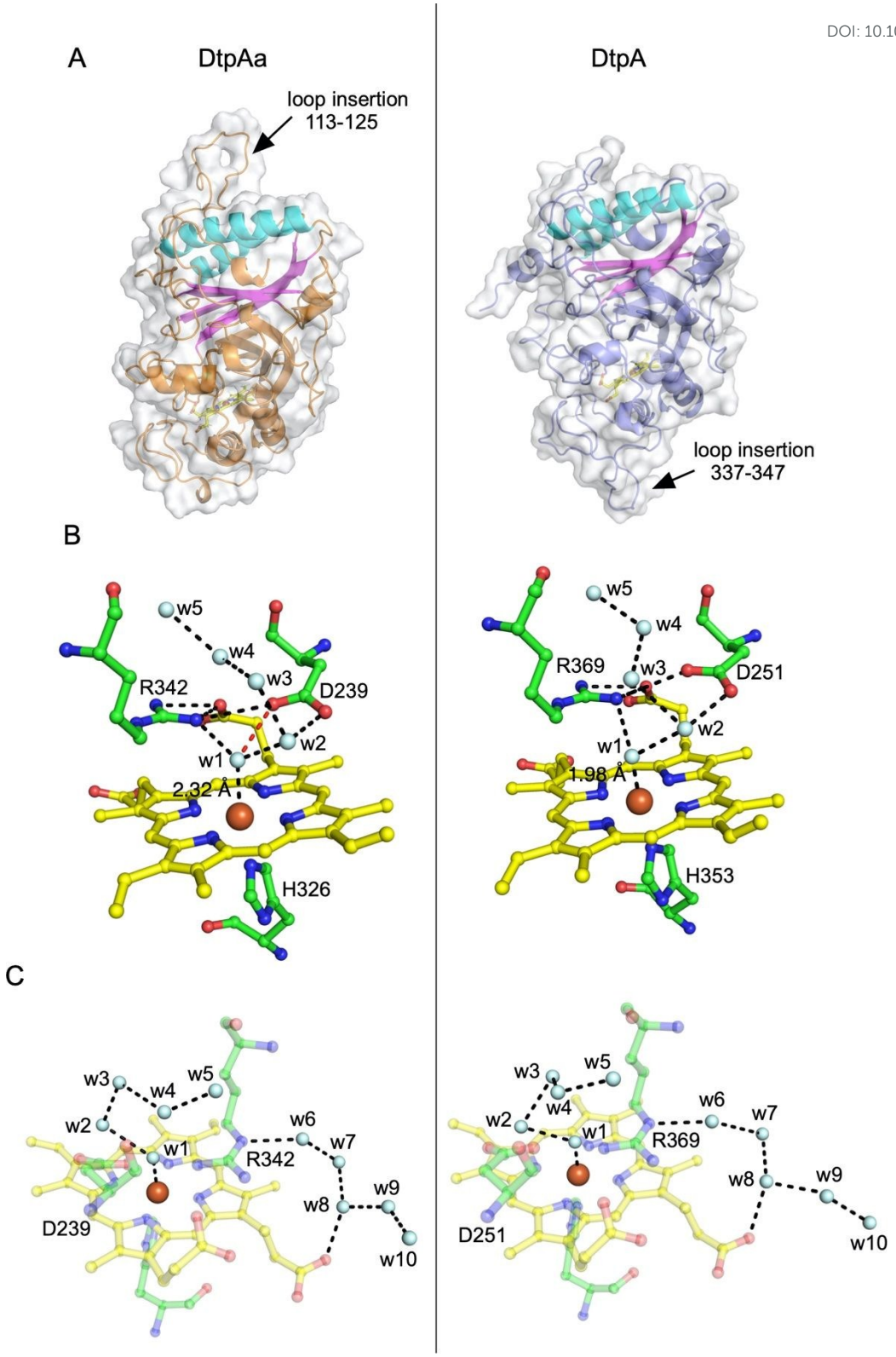

Figure 2: X-ray crystal structures determined at 100 K of DtpAa and DtpA[28] in the ferric haem oxidation state. A) Cartoon of the overall structure and surface representation. The fold for one of the ferredoxin-like domains in each structure is highlighted. B) Haem pocket environment, with H_2O molecules shown as cyan spheres (w). C) Extended H_2O network originating in the distal haem pocket and connecting to the enzyme surface.

View Article Online
DOI: 10.1039/C9DT04583J

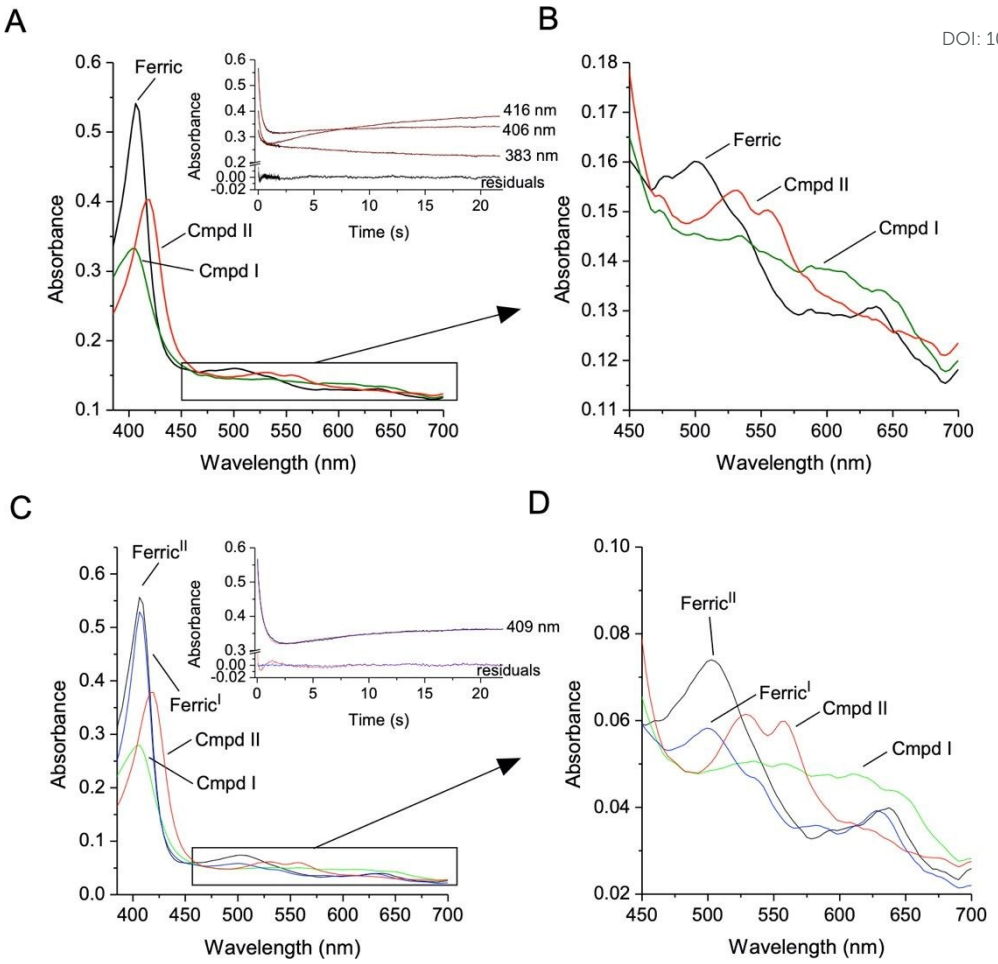

Figure 3: Detection of Compound I (Cmpd I) in DtpAa using stopped-flow absorption spectroscopy (25 °C). Spectra obtained from global fitting of the observed spectral transitions upon mixing H_2O_2 (62.5 μM) with ferric DtpAa (5 μM) at pH 7.0 (A and B) and at pH 5.0 (C and D) according to models described in the main text. The haem species identified by global analysis are labelled. Insets A and C show kinetic traces at the specified wavelengths along with their fits and residuals to models described in the text. The kinetic trace in the inset of (C) has been fitted to two models as indicated by the blue and red residuals (see main text).

View Article Online
DOI: 10.1039/C9DT04583J

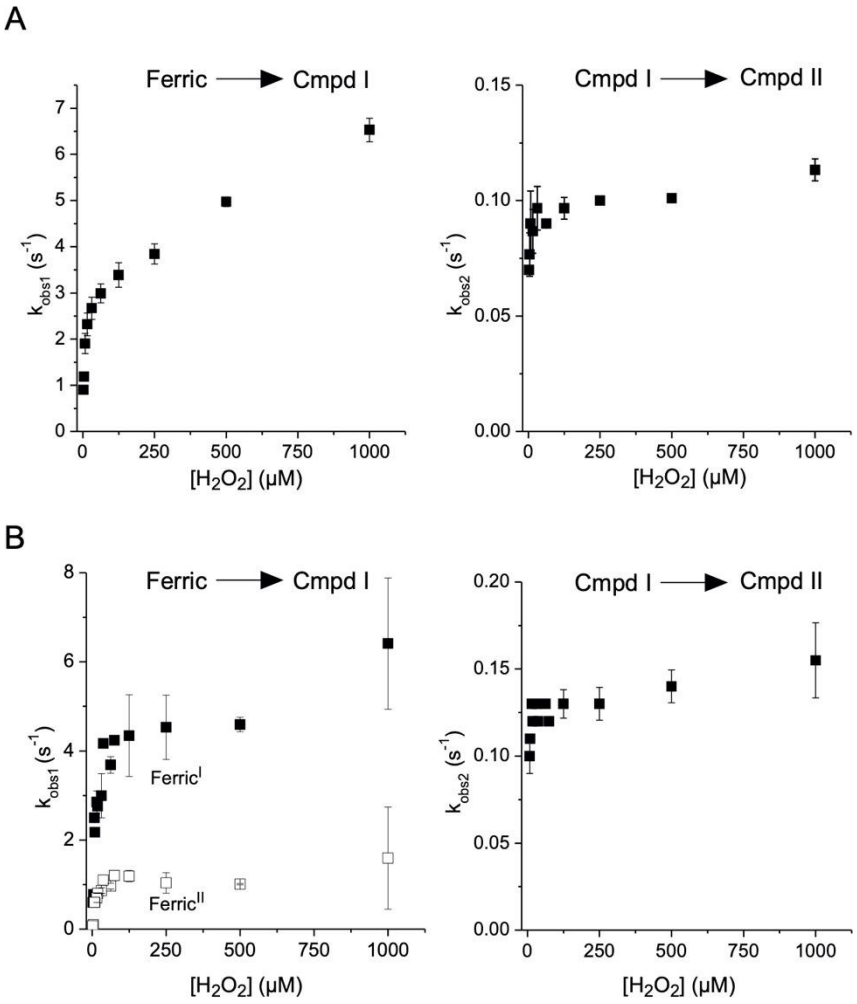

Figure 4: Observed pseudo-first order rate constants (k_{obs1} and k_{obs2}) obtained from global fitting of the spectral transitions for the reaction of DtpAa (5 μM) with increasing H_2O_2 concentrations at pH 7.0 (A) and pH 5.0 (B) at 25 °C. k_{obs1} is assigned to the formation of Compound I (Cmpd I) from the HS ferric species and k_{obs2} is assigned to the formation of Compound II (Cmpd II) from Compound I. At pH 5.0 two HS ferric species, Ferric^{I} and Ferric^{II} exist giving rise to two k_{obs1} rates.

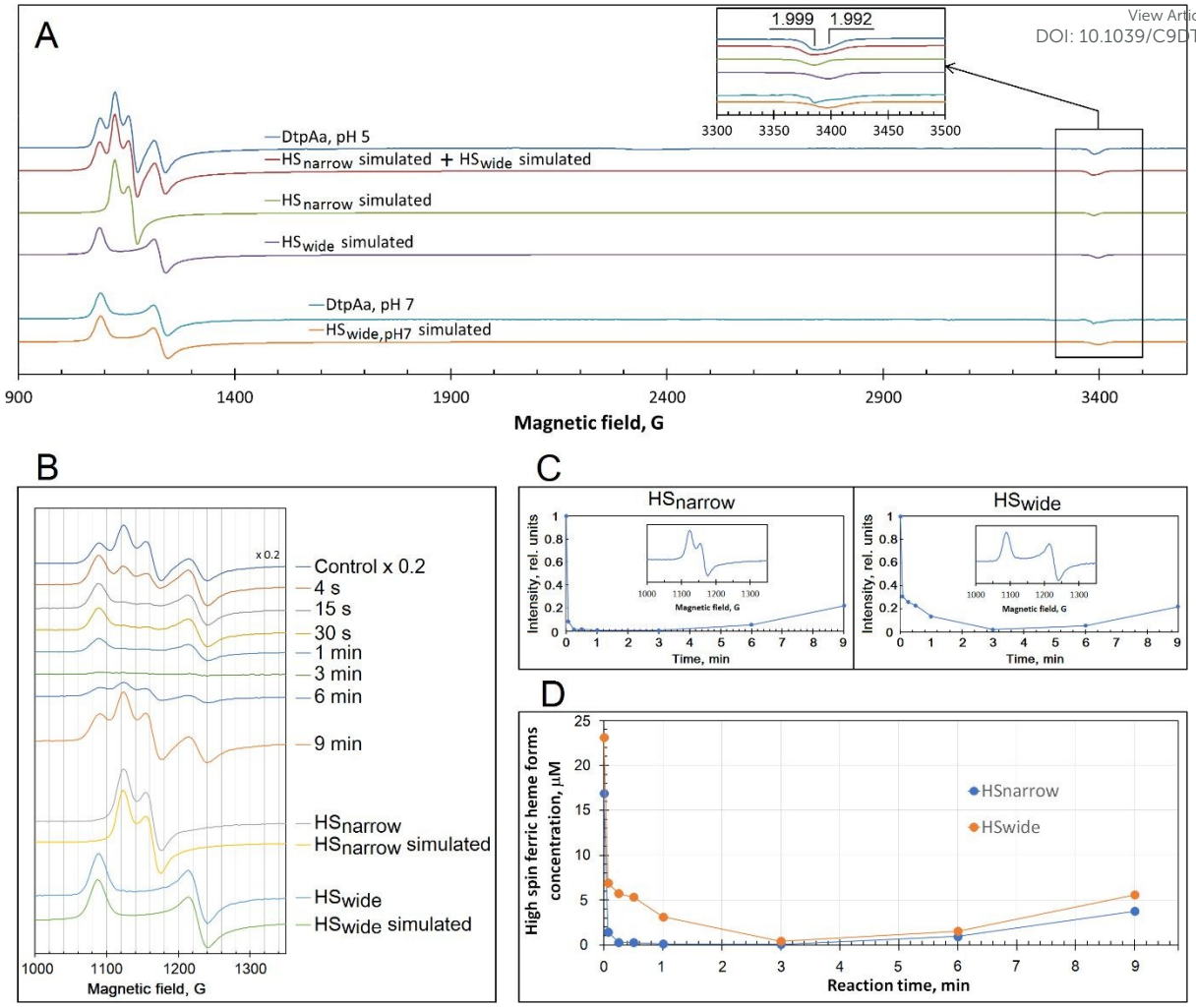

Figure 5: EPR spectroscopy of DtpAa. A) The 10 K EPR spectra of 40 μM DtpAa at pH 5.0 and 7.0 and their simulations. The pH 5.0 spectrum can be represented as a sum of two HS ferric haem signals, whereas the spectrum of DtpAa at pH 7.0 exhibits just one form (further details of the simulated spectra in B and Table 3). B) The change in line shape of the $g_{\perp}$ area of the HS ferric haem EPR signal (g ~ 6) on time following addition of a 10-fold molar excess of H_2O_2 to DtpAa at pH 5. Analysis of the EPR signals allowed extraction of two pure line shapes as follows: HS_{narrow} = {Control} - 3.3x{4 s}; HS_{wide} = {4 s} - 0.084x{Control}. The simulations of these two line shapes (HS_{narrow} simulated and HS_{wide} simulated) have been performed by using the parameters reported in Table 3. C) The kinetics of the two DtpAa HS ferric forms following reaction with H_2O_2 at pH 5.0; the two signals intensities are normalised to 1.00 in the control sample (before addition of H_2O_2). D) The kinetic dependences of the two HS ferric haem forms, as reported in (C), expressed in concentration. Note the sum of the two forms concentrations in the control (t = 0) is 17 μM (HS_{narrow}) plus 23 μM (HS_{wide}), equal to the protein concentration of 40 μM used in the experiment.

View Article Online
DOI: 10.1039/C9DT04583J

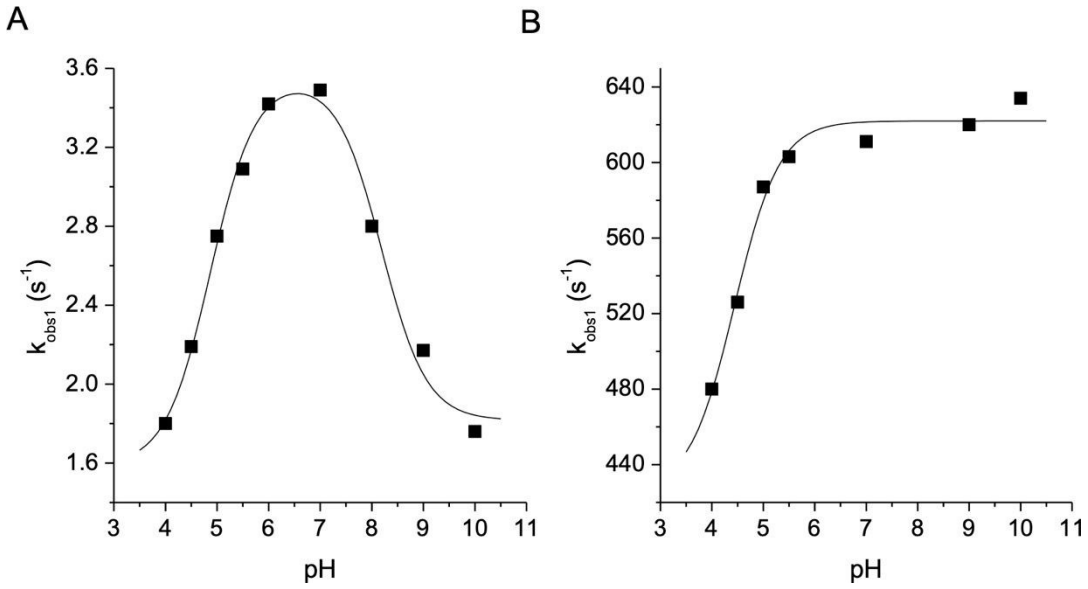

Figure 6: pH dependence profiles for the rate of Compound I formation in DtpAa (A) and DtpA (B) on reacting with a fixed concentration of H_2O_2. Pseudo-first order rate constants (k_{obs1}) were obtained from global fitting of the spectral transitions at a determined pH. For DtpAa (A) the data were fitted to a two-proton ionisation equilibria equation to yield two apparent pK_a's (pK_{a1} and pK_{a2}) and for DtpA (B) an equation for a single-proton ionisation equilibrium was used to yield pK_{a1}. H_2O_2 concentrations used with DtpAa and DtpA are reported in the Experimental section.

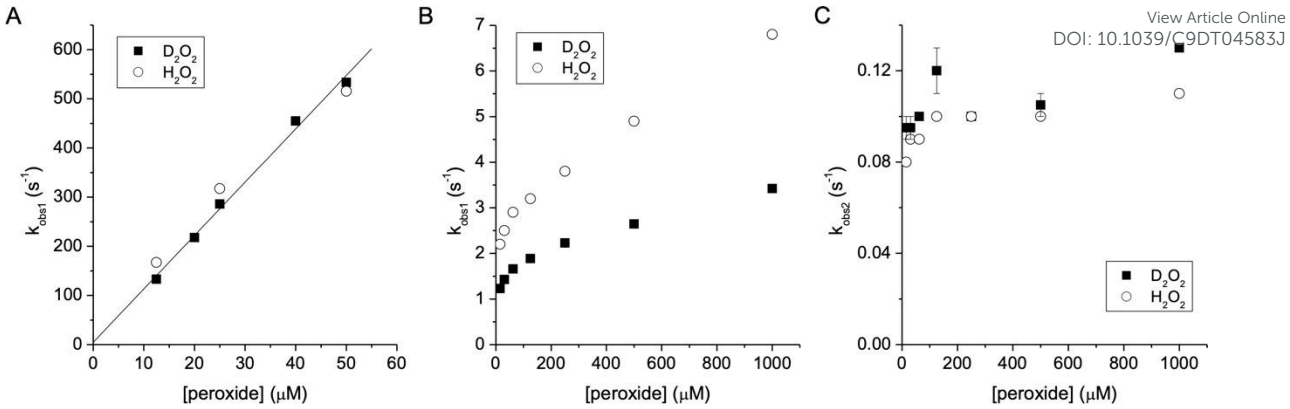

Figure 7: The KIE on the formation of Compound I and Compound II in DtpA and DtpAa at pD 7.0 and 25 °C A) Pseudo first-order rate constants (k_{obs1}) plotted against [D_2O_2] obtained from monitoring the formation of Compound I at 406 nm for DtpA (5 μM). The filled squares (D_2O_2) are fitted to a linear function to obtain a second-order rate constant, and the open circles represent data points at comparative [H_2O_2]. B and C) Pseudo-first order rate constants (k_{obs1} and k_{obs2}) obtained from global fitting of the spectral transitions for the reaction of DtpAa (5 μM) with increasing [D_2O_2] (filled squares) and comparative [H_2O_2] (open circles). k_{obs1} is assigned to the formation of Compound I and k_{obs2} is assigned to the decay of Compound I to Compound II.

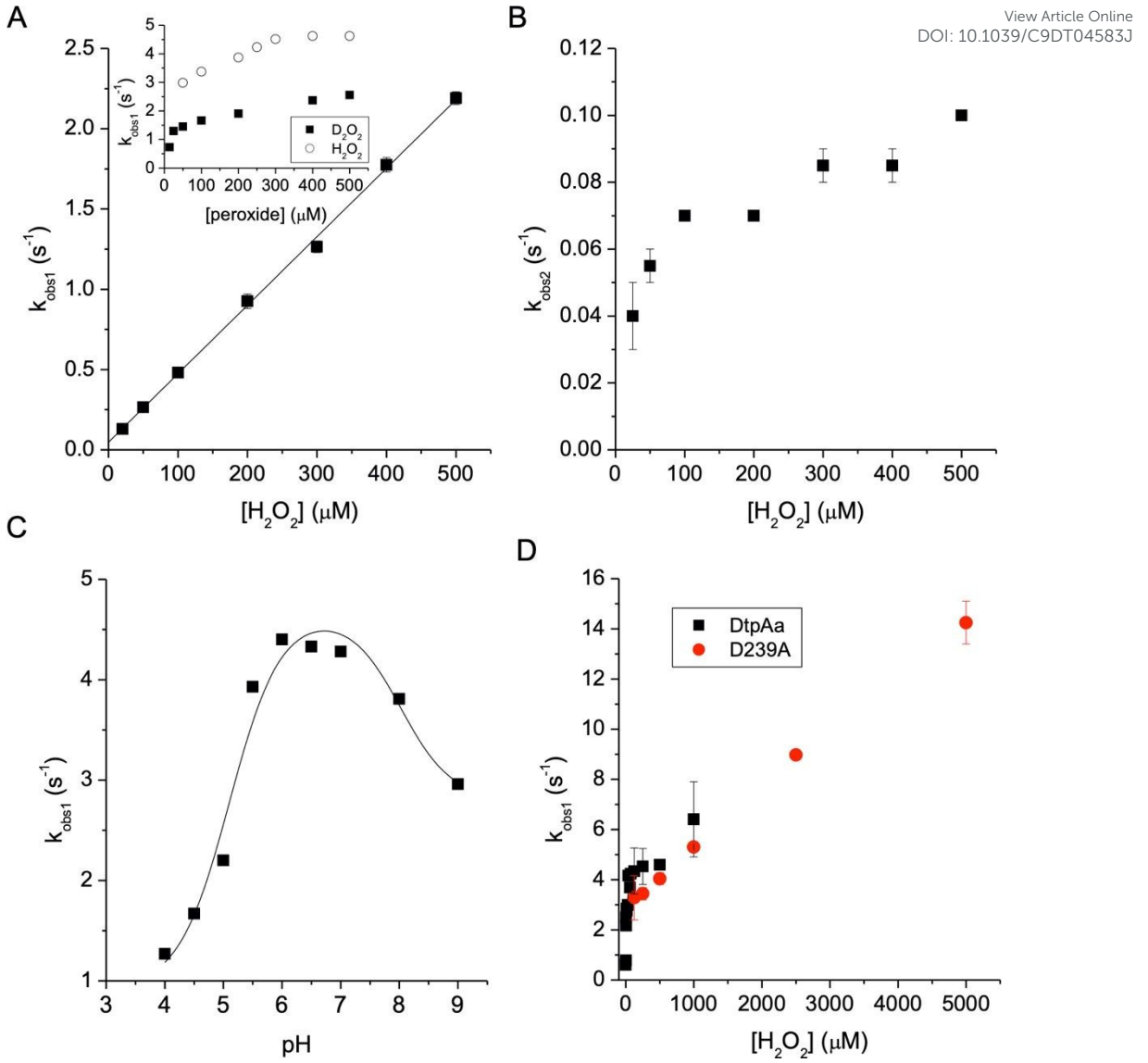

Figure 8: Kinetics of Compound I formation for the distal Asp variants of DtpA and DtpAa at 25 °C. Pseudo first-order rate constants (k_{obs1} and k_{obs2}) were obtained from global fitting of the spectral transitions for the reaction of H_2O_2 or D_2O_2. A) Plot of k_{obs1} values against $[H_2O_2]$ for the D251A variant of DtpA (5 μM) at pH 5.0 and inset pH 7.0. The data points are fitted to a linear function to obtain a second-order rate constant for Compound I formation. B) The k_{obs2} values plotted as a function of $[H_2O_2]$ for the decay of Compound I to Compound II in the D251A variant of DtpA at pH 5.0. C) The pH dependence of Compound I formation for the D251A variant using a fixed $[H_2O_2]$ of 500 μM, with the data fitted to a two-proton ionisation equilibria equation to yield the apparent pK_{a1} and pK_{a2}. D) Overlay of the k_{obs1} values for the D239A variant and wild-type DtpAa at pH 5.0.

View Article Online
DOI: 10.1039/C9DT04583J

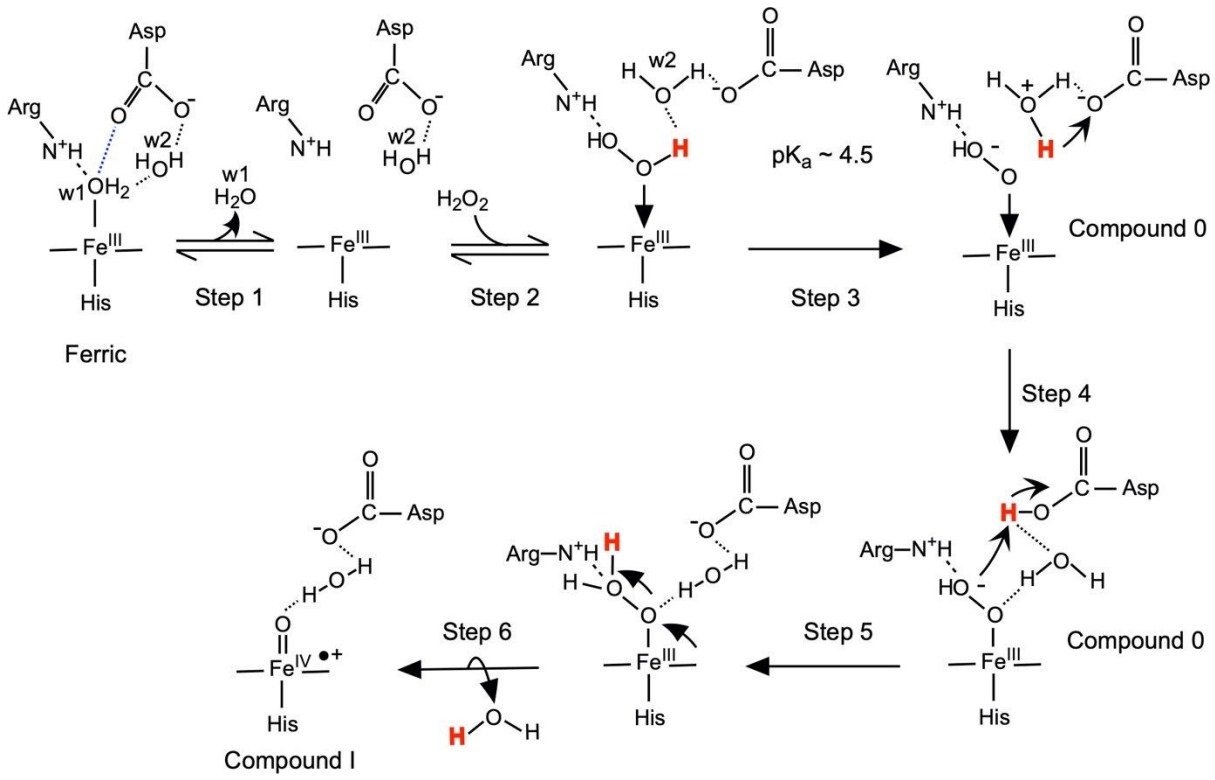

Figure 9: Mechanism of Compound I formation in DtpA and DtpAa. For a description of the individual steps see the main text. The Hα proton of H_2O_2 is depicted in red, and the blue H-bond between the distal Asp and the haem bound H_2O molecule (w1) is only present in ferric DtpAa.

View Article Online
DOI: 10.1039/C9DT04583J

Table of Contents Graphic

A subtle positional shift of the distal haem pocket aspartate in two dye decolourising peroxidase homologs has a remarkable effect on their reactivity with H_2O_2.